Hydrological Processes
Hydrol. Process. **12**, 527–542 (1998)

Evaporation from a riparian system in a semi-arid environment

Helene E. Unland,* Altaf M. Arain, Chawn Harlow, Paul R. Houser,†
Jaime Garatuza-Payan, Paul Scott, Omer L. Sen and W. James Shuttleworth‡
Department of Hydrology and Water Resources, The University of Arizona, Tucson, AZ 85721, USA

Abstract:

Measurements of micrometeorological variables were made for a complete annual cycle using an automatic weather station and two energy budget–Bowen ratio systems at a field site adjacent to the Santa Cruz River in southern Arizona. These data were used to provide the basis of an estimate of the evaporation from a one-mile long losing reach of a riparian corridor in this semi-arid environment. A remotely sensed map of vegetation cover was used to stratify the corridor into five categories of surface cover. The total evaporation was calculated as the area-weighted average of the measured evaporation for sampled areas of the two most common covers, and appropriate estimates of evaporation for the less common covers. Measurements showed a substantial, seasonally dependent evaporation from the taller, deep-rooted riparian cover in the study reach, while the short, sparse vegetation provided little evaporation. In terms of the volume of water evaporated from the study reach, the evaporation from irrigated agriculture accounts for almost half of the total loss, while the majority of the remaining evaporation is from the taller riparian vegetation covers, with about one-quarter of the total loss estimated as coming from obligatory phreatophytes, primarily cottonwood. © 1998 John Wiley & Sons, Ltd.

KEY WORDS evaporation; semi-arid environment; riparian corridor; riparian vegetation; Sonoran Desert; micrometeorological variables

INTRODUCTION

Semi-arid environments cover a substantial portion of the Earth's land surface and, in semi-arid regions, the narrow areas adjacent to continuously flowing streams are havens of life. Such persistent streams are often found where an otherwise deep water table (perhaps sustained by remote mountain-front recharge) intersects the surface. Therefore, the existence of the stream and associated vegetation is marginal because it depends on groundwater and surface water being accessible to the riparian vegetation. Hence, water development projects involving pumping of groundwater can cause the water table to decline and can put vegetation cover at risk (Stromberg *et al.*, 1993). Alternatively, the effluent produced after the use of groundwater may be released into an otherwise dry stream bed to create a new riparian system downstream, which is then recognized as having ecological value.

The Sonoran Desert in the south-western United States is an example of a semi-arid region where heavy groundwater pumping is affecting the pattern and sustainability of riparian systems. In this region, only about 2% of ground area is covered by riparian vegetation (Stromberg *et al.*, 1993). However, there remains

* Now at Coordinación Riego y Drenaje, Juitepec, Morelos 62550, Mexico.
† Now at NASA Goddard Space Flight Center, Greenbelt, MD 20771, USA.
‡ Correspondence to: W. James Shuttleworth.

Contract grant sponsor: NASA
Contract grant number: NAG5-3854, NGT-30303, NAGW-4165.

CCC 0885–6087/98/040527–16$17·50

Received 19 March 1997
Accepted 15 May 1997

a near total lack of knowledge on the evaporative loss of the ecologically important strips of riparian vegetation.

The research reported in this paper was part of a broader study designed to document and model the interaction between surface water and groundwater processes in the riparian corridor of a sample reach of the Santa Cruz River north of Nogales, a city located on the border between Arizona and Mexico. The study focused on a 'losing reach' downstream of the Nogales International Wastewater Treatment Plant. The results reported in this paper relate to measurements made to document the water lost by evaporation from the riparian system under study.

Information on the observational and estimation strategy used to quantify evaporation is given in the next section followed by documentation of the estimated evaporation rates. Field site, measurement theory, instrumentation and data acquisition, handling, and processing are described in the section on field systems.

OBSERVATIONAL AND ESTIMATION STRATEGY

The observational approach used in this study was adopted considering the limitations inherent to the micrometeorological methods used, the diverse nature of the riparian corridor under study, and the availability of instruments and resources. The micrometeorological systems used to measure evaporation can only realistically provide measurements representative of a particular type of vegetation cover when there is a reasonably extensive, uniform area of that vegetation immediately upwind of the instruments. The vegetation cover in the study reach was a diverse mixture of natural covers, irrigated agriculture crops, and retired agricultural areas, while the instrumentation available was limited to two proprietary energy budget–Bowen ratio (EBBR) surface energy flux measuring systems and an automatic weather station.

Given the above limitations, some compromise between practicality and representativeness was essential. The strategy adopted was to assume that the riparian system in the study reach could realistically be considered as comprising one of five different surfaces, these being defined according to the likely distinction in their evapotranspiration loss, thus:

(a) open water surfaces (primarily the river);
(b) areas of irrigated agriculture;
(c) strips of tall vegetation (primarily obligatory phreatophytes, especially cottonwood);
(d) medium/high-density vegetation of medium height (primarily facultative phreatophytes, especially mesquite bosque); and
(e) low-density, short vegetation (the river floodplain and retired agriculture).

The fractional cover area of each of the above classes was estimated by grouping the measured areas of appropriate subclasses of vegetation obtained from a remotely sensed land use map, shown in Figure 1. This map was created by digitizing land use areas from aerial photographs taken in 1990, but the land use areas are believed to be reasonably good approximations to the actual area of each component cover in 1995–1996. Although any change in coverage that may have occurred since 1990 is undocumented, the land use designations reported on the map still appeared to agree well with sample ground-truth observations in 1995. The total areas assigned to each of the five prescribed riparian surface covers used in this study were in some cases obtained by combining some of the component covers defined in the land cover map. The areas of each component surface cover are given in Table I.

The two EBBR evaporation measurement systems were deployed over reasonably large, representative areas of the two most common vegetation covers present in the study reach, namely surfaces (d) and (e), respectively. The evaporation rates for the three remaining cover classes, (a), (b) and (c), were then estimated from routinely measured weather variables using evaporation estimation formulae. It is believed that evaporation rates for covers (a) and (b) can be estimated fairly reliably in this way (see next section), and the area of open water surfaces is in any case comparatively small. Given the current level of uncertainty regarding the evaporation from obligatory phreatophytes, the evaporation from surface cover type (c) was

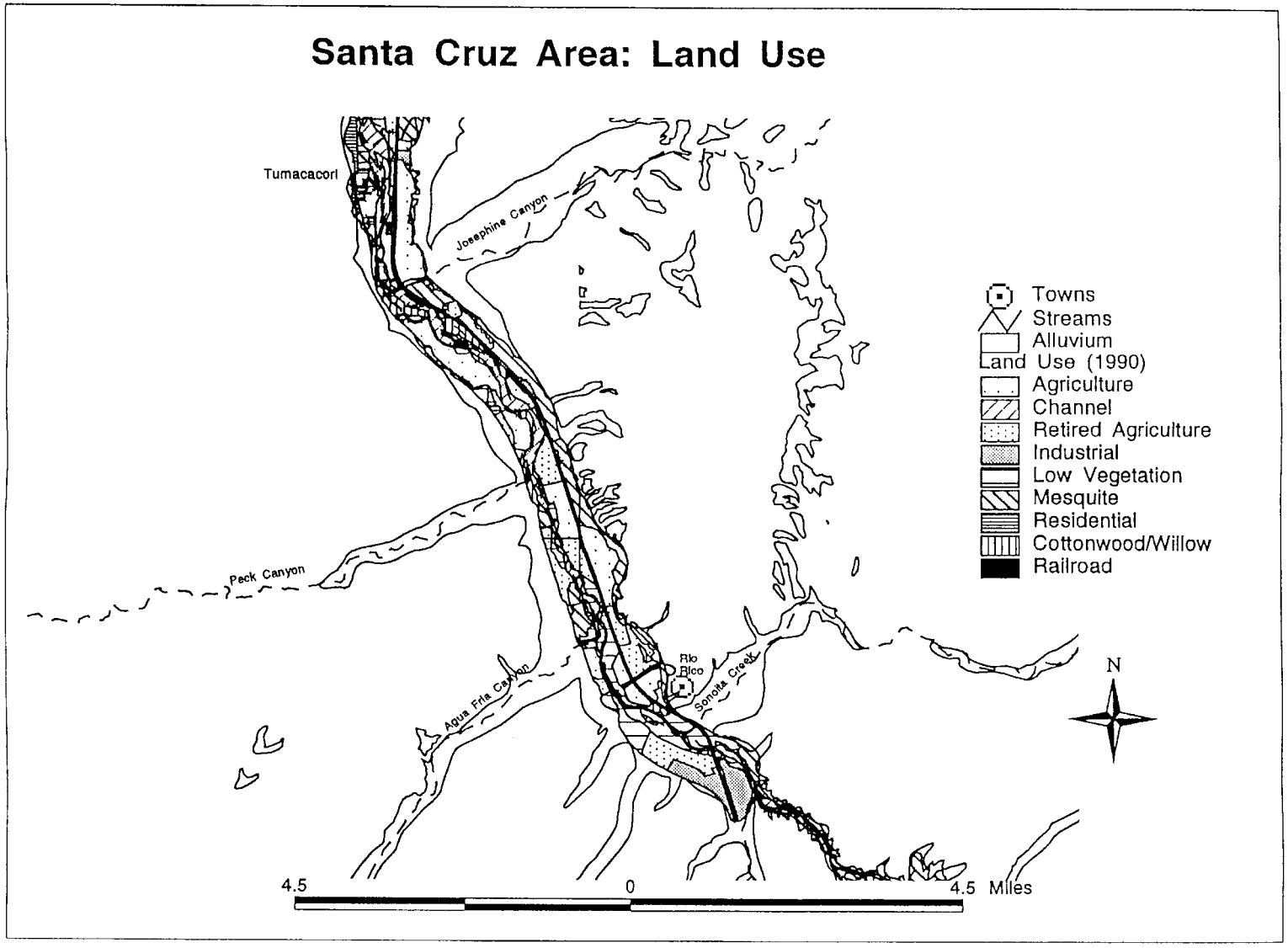

Figure 1. Land cover map for the study reach of the Santa Cruz River (Arizona State University, 1992)

Table I. Cover area of riparian surface covers used in this study

Surface cover class (based on likely evaporation loss)	Map category	Category area (hectare)	Surface cover area (hectare)
Cover (a) (open water surfaces, primarily the river)	(Not applicable)	26·99	26·99
Cover (b) (irrigated agriculture)	Agriculture	433·56	433·56
Cover (c) (obligatory phreatophytes)	Cottonwood/willow	170·56	170·56
Cover (d) (other tall riparian species, primarily facultative phreatophytes)	Mesquite bosque	326·69	326·69
Cover (e) (low density, short vegetation, primarily retired agriculture and the river flood plain)	Low vegetation	663·98	663·98
Other (not considered in this study)	Industrial	23·75	90·49
	Low density residential	7·63	
	Transportation	59·10	

Note: the area of cover (a) was estimated from the length of the study fetch and an estimated average width of the river

deliberately overestimated in this study (see later). The calculated evaporation rates for the whole riparian system are likely to be biased slightly high (and any ensuing estimate of groundwater recharge presumably biased slightly low) for this reason. In practice, however, the resulting error in the total evaporation from the entire riparian system in the study reach is limited by the fact that this is just one of the several covers present (see later).

ESTIMATED EVAPORATION RATES

Evaporation from open water surfaces

Evaporation from exposed, open water surfaces is usually considered to be well estimated by the so-called *potential evaporation rate*, this being defined as the quantity of water evaporated per unit area, per unit time from an idealized, extensive free water surface under existing atmospheric conditions. The recommended equation to estimate the potential evaporation rate, E_p, from measured meteorological variables (Shuttleworth, 1993) is that due to Penman (1948), which has the form:

$$E_p = \frac{\Delta}{\Delta + \gamma}(R_n - A_h) + \frac{\gamma}{\Delta + \gamma}\frac{6{\cdot}43(1 + 0{\cdot}536U_2)D}{\lambda} \quad (1)$$

where R_n is the net input of radiant energy to the water surface, expressed as the equivalent evaporation rate in mm day^{-1}, A_h is the energy carried in the flowing water (if significant), expressed as the equivalent evaporation rate in mm day^{-1}, U_2 is the wind speed measured at 2 m, in m s^{-1}, D is the vapour pressure deficit of the air, in kPa, λ is the latent heat of vaporization of water, in MJ kg^{-1}, Δ is the gradient of saturated vapour pressure curve at air temperature, in kPa °C^{-1}, and γ is the psychrometric 'constant', in kPa °C^{-1}. The variables λ and Δ are known functions of the measured temperature, while the psychrometric constant $\gamma = 0{\cdot}0016286\ (P/\lambda)$, where P is air pressure in kPa.

Two features influence how well this potential evaporation rate estimates evaporation from the river surface. First, the estimated potential rate is strictly relevant to extensive areas of evaporating water surface. Area-average evaporation rates from smaller areas of water, such as a narrow river, tend to be higher by (say) about 10%, because it is easier to advect energy in the moving air to enhance evaporation. Secondly, the

calculated potential evaporation rate assumes that all of the water surface (in this case, the river) is fully exposed to the radiant energy from the sun. In fact, portions of the Santa Cruz River are shaded by overhanging trees and, consequently, the actual evaporation from the river in the study reach will tend to be less than the potential rate. There will no doubt be some compensation between these two opposing factors, but it is likely that the influence of shading the river surface will dominate and that the estimated rate of evaporation from the river surfaces might be biased high, perhaps by as much as 10–20%.

Evaporation from irrigated crops

Evaporation from short, well-watered grass is considered to be well estimated by the so-called *reference crop evaporation rate*, defined as the quantity of water evaporated per unit area, per unit time from an idealized crop with a fixed height of 0·12 m, an albedo of 0·23 and a surface resistance of 69 s m^{-1} (Shuttleworth, 1993). The recommended equation to estimate the reference crop evaporation rate, E_{rc}, from measured meteorological variables (Shuttleworth, 1993) has the form:

$$E_{rc} = \frac{\Delta}{\Delta + \gamma^*}(R_n - G) + \frac{\gamma}{\Delta + \gamma^*}\frac{900}{T + 275}U_2 D \tag{2}$$

In Equation (2), the variables are those used to calculate the potential evaporation rate [see Equation (1)] except G which is the flux of heat into the soil, expressed as the equivalent evaporation rate in mm day^{-1}. The net input of energy into the soil over the course of a day is usually small because most of the energy entering the soil during the day subsequently leaves during the night. This small term was neglected in this study. The 'modified psychrometric constant', γ^*, in Equation (2) is given by:

$$\gamma^* = (1 + 0{\cdot}33U_2) \tag{3}$$

The evaporation rate from well-watered crops and moist soil can differ from that of a reference crop of well-watered grass. Typically, differences are of the order of 10–20% (e.g. Shuttleworth, 1993), either higher or lower depending on the crop. The remotely sensed map of vegetation cover used in this study classified agriculture only as active (and irrigated) or retired (and not irrigated). Therefore, it was not possible to distinguish between the rates of evaporation for the different irrigated crops involved in the actively farmed areas of irrigated agriculture. However, this is actually a realistic and sensible approach to adopt because the precise nature of individual crops will change with time at any particular location. The evaporation loss from all of the irrigated crops in the study reach was assumed equal to that of a short, well-watered, grass reference crop. In practice, there will be periods when there is less than complete vegetation cover at some irrigated sites, which will tend to reduce the local evaporative loss during such periods. Hence, it is possible that the estimated evaporation for the irrigated proportion of the study reach might again be biased high, by (say) 20%.

Evaporation from obligatory phreatophytes

At the time of writing, there is considerable uncertainty and controversy regarding the evaporation from obligatory phreatophytes (especially cottonwood). Given this controversy (which centres around the suggestion that cottonwood evaporation rates are often systematically underestimated), a decision was taken to err on the side of overestimating, rather than underestimating, the evaporation rate for the obligatory phreatophytes present in the study reach. Fortunately, the overall effect of making this deliberate overestimate on the estimated evaporation loss for the entire riparian system in the study reach is moderated by the fact that this vegetation cover is just one of several present.

Gatewood *et al.* (1950) estimated cottonwood evaporation flux to be roughly twice that of mesquite in Safford Valley, Arizona. Consistent with this result, and bearing in mind the intention to err on the side of overestimation, the estimated evaporation rate for areas of obligatory phreatophytes, cover class (c), was arbitrarily assumed to be twice the measured rate of evaporation for facultative phreatophytes, that is, twice the rate of cover class (d).

FIELD SYSTEMS

All of the evaporation estimates described above require measured values of the meteorological variables used in the respective estimation formulae. An automatic weather station was installed at the field site to make the required measurements. The direct measurements of evaporative loss from facultative phreatophytes [cover class (d)] and low-density, short vegetation [cover class (e)] were also made at this same field site using micrometeorological instrumentation.

Experimental site

The study site is located within the Upper Santa Cruz Valley near the confluence of Agua Fria Canyon and the Santa Cruz River (31°28′45″N and 110°59′48″W). It is approximately 90 km south of Tucson, 16 km north of Nogales, Arizona, and about 4 km north-east of the Nogales International Waste Water Treatment Plant. A location map of the field site is given in Figure 2 along with a sketch showing the relative position of the main instrumental systems relative to the Santa Cruz River and the surrounding vegetation.

The climate of the Santa Cruz Valley is semi-arid, with temperatures (recorded at Nogales) ranging from −3 °C to 35 °C and an annual average temperature of 16 °C. Precipitation has a bimodal seasonal pattern, with most rain falling during a summer monsoon season (in July and August) but some in the winter season (in December and January). The summer storms produce heavy convective rainfall, while winter precipitation, which comes from frontal systems, tends to be more widespread and have lower intensity. Annual rainfall in the valley is usually around 400–500 mm.

Mesquite bosque [cover class (d)] is the most common vegetation at the study site, but other species are also present, specifically willow (*Salix gooding*), *Sambucus mexicana*, *Celtis reticulata*, and occasional cottonwood [cover class (c)]. Some of the cottonwood trees are 12 m tall. A cattle-grazed pasture and a cultivated field are located south-west of the site. The areas along the banks of the Santa Cruz River, which are prone to regular flooding, are sparsely covered with short shrubs and grasses with large areas of exposed soil. The vegetation greenness peaks in the monsoon season (July–September), and the trees have minimum canopy cover in winter (November–March). However, *Celtis reticulata*, which is sparsely scattered throughout the primarily mesquite bosque stand at the site, is always green.

Instrumentation and methods

Two towers were installed at the field site, one over the tall riparian vegetation corresponding to cover class (d) and the second in the area with short shrubs, grass and bare soil, corresponding to cover class (e). The 12-m high tower located over the dense mesquite bosque was 137 m west of the Santa Cruz River (Figure 2). Instrumentation installed on this tower included an automatic weather station and one of the two EBBR systems used to measure evaporation. The second Bowen radio system was installed on a 6·25-m high tower, which was erected about 46 m west of the Santa Cruz River in the flood-prone region with low vegetation.

Automatic weather station. The automatic weather station provided continuous measurements of net radiation using a net radiometer (REBS, Washington); incoming short-wave radiation using a pyranometer (Licor, Kansas); air temperature and relative humidity using a temperature/RH probe (Vaisala, Finland); wind speed and wind direction, using an anemometer and a wind vane (Campbell Scientific, Utah); and soil temperatures and heat flux, using four soil thermocouple probes and two soil heat flux plates (Campbell Scientific, Utah). These measurements were recorded on a 21X data logger (Campbell Scientific, Utah) as 15-minute average values and were later combined to give hourly average values.

The net radiation was recorded on the 12-m tower at a height of 8·23 m, short-wave radiation at 11·7 m, and air temperature and relative humidity at a height of 7·92 m. The anemometer and wind vane were installed at 12·19 m. Precipitation was measured using a tipping-bucket rain gauge (Texas Electronics, Texas) located at a well-exposed site close to the second tower in the sparse vegetation (Figure 2).

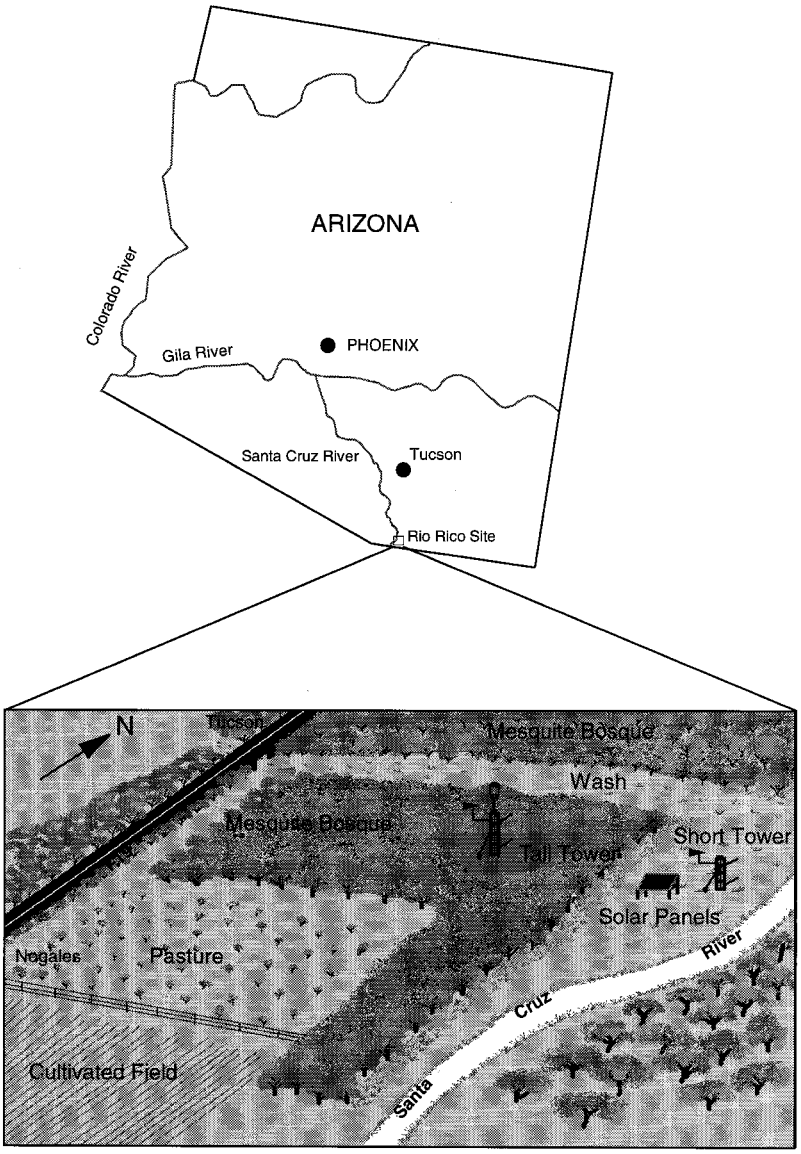

Figure 2. Location map and schematic arrangement of the Rio Rico field site in the Upper Santa Cruz River Valley in southern Arizona

Bowen ratio–energy budget systems. The energy budget–Bowen ratio (EBBR) method relies on measuring the components of the surface energy budget:

$$R_n - G = H + \lambda E \tag{4}$$

where the net radiation, R_n, and the soil heat flux, G, are directly measured, while the ratio of λE (latent heat flux) and H (sensible heat flux), the so-called Bowen ratio, β, is estimated from measurements of the difference in vapour pressure, de, and potential temperature, dT, between two levels above the ground using the equation:

$$\beta = \frac{H}{\lambda E} = \left(\frac{c_p P}{\varepsilon \lambda}\right)\left(\frac{\mathrm{d}T}{\mathrm{d}e}\right) \tag{5}$$

where c_p is the specific heat of air (in kJ kg^{-1} °C^{-1}), and ε (0·622) is the ratio of molecular weight of water relative to that of air.

Combining Equations (4) and (5) gives:

$$\lambda E = (R_n - G)\left[1 + \left(\frac{c_p P}{\varepsilon \lambda}\right)\left(\frac{dT}{de}\right)\right]^{-1} \tag{6}$$

with the sensible heat flux then derived as the residual in the energy balance equation, thus:

$$H = R_n - G - \lambda E \tag{7}$$

One EBBR system (Campbell Scientific, Utah) was installed on each of the two towers at the field site. These systems recorded data initially as 20-minute averages. Two 1·5-m long arms were mounted to extend from both towers, at 6·28 m and 11·59 m in the case of the tall tower, and at 3·05 m and 6·10 m in the case of the short tower. The difference in air temperature between these two arms was measured using 0·075-mm diameter chromel–constantan thermocouples located at the end of each of the arms. The difference in vapour pressure was measured by ducting air from filtered air intake ports located on each arm (about 0·75 m out from the tower) via polyethylene tubing and a 2-litre polyethylene 'buffering' container to a DEW-10 cooled dew point hygrometer. The dew point hygrometers alternately sampled the humidity content of the air from the two air intakes on the towers.

The net radiation measurements required for the energy budget–Bowen ratio flux calculations were available from the automatic weather station for the tall vegetation and from a second Q-7 net radiometer mounted just south of the short tower for the short, sparse vegetation. The ground heat flux near each of the towers was obtained as an average of measurements made using four soil heat flux plates buried 8 cm below the soil surface. The precise location of these soil heat flux plates was chosen to sample the mix of bare soil and vegetation at each site. The average soil temperature above the heat flux plates was found by averaging soil thermocouple measurements made at 2 and 6 cm above the soil heat flux plates. The soil heat flux in the surface was then estimated by adding the measured heat flux to the change in energy stored in the layer of soil above the heat flux plates, the latter being proportional to the rate of change in soil temperature.

Aerodynamic measurements of surface fluxes. There are periods of time when measurements made with the energy budget–Bowen ratio method are not considered reliable, especially when the Bowen ratio is either close to -1 or when the latent heat flux and hence the difference in vapour pressure between the two measurement levels is small and, consequently, the fractional measurement error in de is large. On such occasions, the surface fluxes were measured using the aerodynamic method. The mathematical framework for the aerodynamic method has been described in detail by Brutsaert (1982), and only the final equations are given here. In these equations, the stability factors used are suggested by Dyer and Hicks (1970) in unstable and neutral atmospheric conditions, and by Webb (1970) in stable atmospheric conditions.

In the aerodynamic method, the latent heat flux and the sensible heat flux are calculated from the equations:

$$\lambda E = [(de.k.u_*.\rho.\varepsilon)/P]\{\ln[(z_2 - d)/(z_1 - d)] - \psi_{H,V}(z_2) + \psi_{H,V}(z_1)\} \tag{8}$$

$$\mathrm{H} = [dT.k.u_*.\rho.c_p]\{\ln[z_2 - d)/(z_1 - d)] - \psi_{H,V}(z_2) + \psi_{H,V}(z_1)\} \tag{9}$$

where z_1 and z_2 are the upper and lower measurement heights, respectively; k (= 0·4) is von Karman's constant; ρ is the density of air; and u_* is the friction velocity given by:

$$u_* = \frac{(u_z.k)}{\ln[(z_u - d)/z_0) - \psi_M(z_u)]} \tag{10}$$

where u_z is the wind speed measured at height z_u, and z_0 and d are the roughness length and zero plane displacement of the underlying surface, respectively. The empirical functions $\psi_{H,V}$ and ψ_M depend on atmospheric stability, as follows. In unstable and neutral conditions, when $[(z_u - d)/L]$ is less than or equal to zero, they are:

$$\psi_{H,V}(z_1) = 2 \ln\left\{\frac{[1 + f(z_1)^2]}{[1 + f(z_0)^2]}\right\}$$

$$\psi_{H,V}(z_2) = 2 \ln\left\{\frac{[1 + f(z_2)^2]}{[1 + f(z_0)^2]}\right\}$$

$$\psi_M(z_u) = \ln\left\{\frac{[1 + f(z_u)]^2[1 + f(z_u)^2]}{[1 + f(z_0)]^2[1 + f(z_0)^2]}\right\} - 2 \arctan[f(z_u)] - 2 \arctan[f(z_0)]$$

where

$$f(z) = [1 - 16(z - d)/L]^{0.25}$$

In stable conditions, when $[(z_u - d/L]$ is greater than zero but less than unity, they are:

$$\psi_{H,V}(z) = -5{\cdot}2(z - z_0)/L \quad [z = z_1 \text{ or } z_2]$$
$$\psi_M(z_u) = -5{\cdot}2(z_u - z_0)/L$$

but when $[(z_u - d)/L]$ is greater than unity, it is assumed that:

$$\psi_{H,V}(z_1) = \psi_{H,V}(z_2) = \psi_M(z_u) = -5{\cdot}2$$

In the above equations, L is the Monin–Obukov stability length given by:

$$L = -[\rho u_*^3]\{kg[H/(c_p T) + 0{\cdot}61\lambda E]\}^{-1}$$

in which T is the air temperature (in K) and g is the acceleration due to gravity. Because the value of L is required to calculate H and λE from the above equations, it is necessary to solve for them by iteration, starting with $H = 0$ and $\lambda E = 0$ and then recalculating L after each iteration cycle until consistency is achieved, i.e. until the change in H and λE during the last iteration is less than 0·1 Wm^{-2}. In practice, the iteration algorithm can sometimes fail to converge (in 300 iterations). This is especially true for low wind speeds ($u_z < 1$ m s^{-1})), because $L \propto u_*^3$ and small changes in the value of u_* can cause large changes in L.

The wind speed used in these calculations was recorded on the tall tower. Its value was extrapolated downwards assuming a logarithmic wind profile to 6·1 m for use in calculating the aerodynamic flux calculations for the short tower. The effective values of the roughness length and the displacement height used in the calculations for the tall vegetation [cover class (d)] were 0·25 and 2·25 m, respectively, while for the short, sparse vegetation [cover class (e)], they were 0·1 and 0·75 m, respectively.

Selecting the preferred measurement method

When estimates of surface fluxes were available from both the energy budget–Bowen ratio method and the aerodynamic method, a choice between them was made on the basis of the estimated error in the value of the latent heat flux. This error would result from a measurement error in the vapour pressure difference between the two measurement heights. If the error in the calculated latent heat flux is $\delta_{\lambda E}$, then it can be shown by a

propagation of error calculation that, for the EBBR method, the contribution to $\delta_{\lambda E}$ given by an error Δe in the measured vapour difference is such that:

$$\left|\frac{\delta_{\lambda E}}{\Delta e}\right|_{\text{Bowen ratio}} = \left|\frac{(R_n - G)\gamma \mathrm{d}T}{(\mathrm{d}e + \gamma \mathrm{d}T)^2}\right|$$

In the case of the aerodynamic method, the equivalent expression is:

$$\left|\frac{\delta_{\lambda E}}{\Delta e}\right|_{\text{Aerodynamic}} = \left|\frac{\varepsilon k u_* \rho \lambda}{P\{\ln[(z_2 - d)/(z_1 - d)] - \psi_{H,V}(z_2) + \psi_{H,V}(z_1)\}}\right|$$

These two ratios were evaluated for measurement periods when both methods were available, and the measurement method giving the smaller value of $|\delta_{\lambda E}/\Delta e|$ was then selected for that period.

Site-related limitations on data quality

The surface areas contributing to the fluxes measured using micrometeorological techniques do not necessarily correspond to those for the underlying vegetation cover. In principle, there is always some contribution from all areas upwind of the instruments, with the relative contribution falling off with distance from the tower. In practice, such contamination can easily be significant for measurements over riparian stands because of their very heterogeneous nature and the comparatively small patches of vegetation that usually make up the riparian system.

An estimate was made of the surface area contributing to the micrometeorological flux measurements using the approach of Schuepp *et al.* (1990) and Desjardins *et al.* (1992) applied with aerodynamic parameters and instrument heights appropriate for this field site. In the calculation, the values assumed for the roughness length and the zero plane displacement height for the tall tower were 0·25 and 2·25 m, respectively, and for the short tower were 0·1 and 0·75 m, respectively. For the tall tower, 80% of the flux measured at the position of the upper Bowen ratio arm is calculated to originate within 677 m of the tower, but the maximum contribution comes from vegetation within 76 m (the distances calculated for the lower arm are significantly less than this). Similarly, 80% of the flux measured for the upper Bowen ratio arm on the short tower originates within 455 m, with the maximum contribution coming from vegetation within 51 m. These calculations suggest that contamination of the measured fluxes from surface covers other than those above which the instruments were mounted could well be of the order of 20%.

Occasionally, the irrigated field adjacent to the field site became flooded and the water flowed towards the tall tower, making two small ponds, one 50 m south of the tower with an area of approximately 30 m^2 and another about 20 m north-east of the tower with an area of about 50 m^2. This flooding may have enhanced the measured evaporation when it occurred (although its influence was never obvious in the data).

Instrument-related limitations on data quality

In this paper, the data are reported from 1 January 1995 to 31 March 1996 (455 days) for the tall tower, and from 7 March 1995 to 31 March 1996 (390 days) for the short tower. There were missing data throughout these periods for both systems arising from system maintenance, various mechanical failures, and other system limitations.

When operating in a semi-arid environment, the cooled dew point hygrometer is the most troublesome component of this particular Bowen ratio measuring system. Under conditions of very low humidity, it is common to encounter values of dew point outside the operating range of the instrument. Moreover, the device sometimes failed to sense that the dew point had been reached during a cooling cycle, and the heat pump continues to cool the mirror, causing persistent ice formation.

A deliberately exacting set of criteria was applied to select between the Bowen ratio data to ensure their credibility, the primary exclusion being to ignore data when the observations were considered beyond the

instrumental accuracy of the Bowen ratio system as a whole or the accuracy of the individual sensors involved in that system. Accordingly, observations of Bowen ratio for which the absolute value of the vapour pressure difference between the two measurement levels, $|de|$, was less than 0·005 kPa were excluded, as were observations for which the Bowen ratio was close to -1, specifically for the range $|1 + \beta| < 0{\cdot}4$. (Note: the latter condition occurs routinely for short periods around dawn or dusk when the energy available for evaporation is low, sensible and latent heat fluxes are in opposite directions and approximately equal, and the Bowen ratio method cannot determine the size of the two fluxes.) In addition, data for which the latent heat flux was negative when the relative humidity was less than or equal to 80% were considered invalid. This simple plausibility test proved effective in removing spurious data associated with settling periods after instrumental servicing or with one or more of the several modes of instrumental failure described above.

Of the 455-day period (1 January 1995 to 31 March 1996) for which data were analysed for the tall tower, only 46% of the evaporative flux data provided by the energy budget–Bowen ratio system were considered reliable after applying the above rejection criteria and after eliminating times when there was mechanical failure. Similarly, of the 390-day period (7 March 1995 to 31 March 1996) for which data were analysed for the short tower, only 12% of the energy budget–Bowen ratio data were considered reliable. The Bowen ratio system at this tower was unable to measure an accurate Bowen ratio most of the time because the latent heat fluxes were typically very low. However, in many cases when the Bowen ratio measurement was unreliable, it was possible to substitute a reliable evaporation measurement using the aerodynamic method (see earlier). The percentage of valid evaporative flux data from the short tower was, for example, increased to 68% when measurements made with the aerodynamic method were included along with those from the energy budget–Bowen ratio method.

When the hourly average values of micrometeorological data and energy fluxes were calculated, the average was considered unreliable if two (out of the four) 15-minute data values were missing. Similarly, daily average values of energy fluxes were considered invalid if more than 50% of the hourly average data were missing. The missing values of daily average energy fluxes were linearly interpolated from the preceding and subsequent daily average values.

RESULTS

Climate

The observations of near-surface weather variables provided by the automatic weather station confirm that the Rio Rico field site has a typical semi-arid climate. Daily average values of incoming solar radiation, net radiation, air temperature, precipitation, relative humidity, and wind speed are shown in Figure 3. Daily average incoming solar radiation ranges from around 350 Wm^{-2} in the summer to around 180 Wm^{-2} in the winter, with occasional cloudy days having much less than this. Net radiation is lower (typically 75 to 150 Wm^{-2} less) than incoming solar radiation because the often clear skies ensure that substantial energy is returned to the atmosphere in the form of net long-wave radiation. Daily average air temperature varies from 30 °C in the summer to 10 °C in the winter, but the maximum daytime air temperature reaches 40 °C on a typical midsummer day. The annual average value of air temperature for 1995 was 16·5 °C. The wind speed is very low in this valley (except during summer storms), and the annual average value of wind speed for 1995 is only 2·2 ms^{-1}.

Most of the precipitation fell during the monsoon season in July–August. The total precipitation recorded at this site during 1995 was 714 mm, with the highest monthly total of 284 mm falling in August. The daily average relative humidity is as low as 30% during dry periods (midday values are less than half of this), but relative humidity increases to 80% during periods with rain. The annual average value of relative humidity for 1995 is 48·6%.

Measured evaporation fluxes

The monthly average values of the net radiation, sensible heat, latent heat, and soil heat fluxes measured on the tall tower [i.e. over surface cover (d)] for each month from 1 January 1995 to 31 March 1996 are displayed

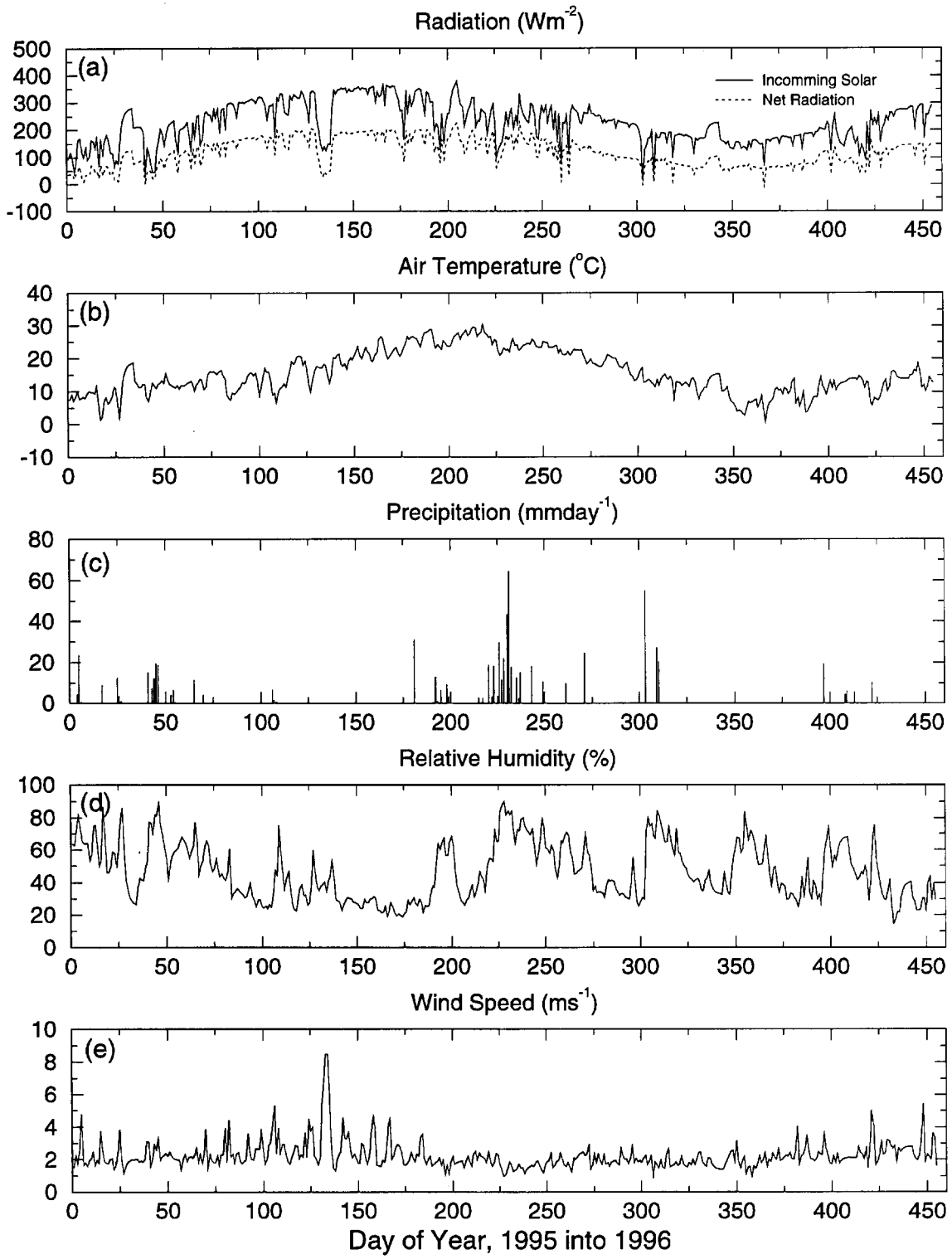

Figure 3. Daily average incoming solar radiation, net radiation, air temperature, total precipitation, relative humidity, and wind speed measured by the automatic weather station from 1 January 1995 to 31 March 1996

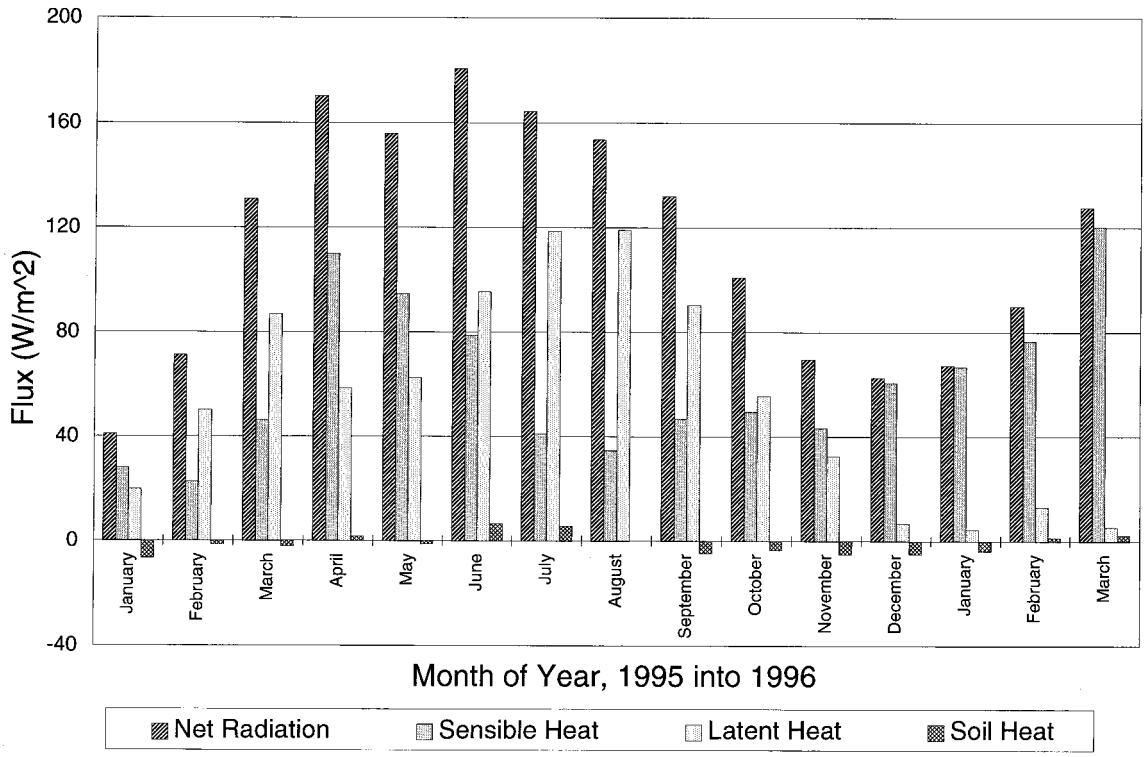

Figure 4. Monthly average values of energy fluxes measured at the tall tower at the Rio Rico field site from January 1995 to March 1996

in Figure 4. The net input of radiant energy for this taller surface cover ranges from around 180 Wm^{-2} in the summer to around 60 Wm^{-2} in the winter. About 70–80% of this radiation is used to evaporate water when rainfall and soil moisture are plentiful. However, in periods of soil moisture shortage, such as in December 1995 and January 1996, only about 10% of the incoming radiant energy is used in this way. There is a small yearly cycle in soil heat flux with an amplitude of around 5 Wm^{-2}, with energy entering the soil in the summer and leaving in the winter. Therefore, the yearly pattern in sensible heat flux loss is largely determined by the surface energy balance between the net radiant energy input and the energy lost as latent heat. In practice, there is a substantial loss of energy as sensible heat in all seasons, with peak values occurring just before the summer and winter rains.

The monthly average values of net radiation, sensible heat, latent heat, and soil heat fluxes measured on the short tower over surface cover (e) from 7 March 1995 to 31 March 1996 are given in Figure 5. The net input of radiant energy to this sparse vegetation cover ranges from about 120 Wm^{-2} in May and June to about 50 Wm^{-2} in December and January. There is a substantial difference in the energy captured by this sparsely vegetated surface compared with that for taller, dense vegetation. Presumably, this is in part because of enhanced reflection of incoming solar radiation by the more exposed (often dry) soil and in part because the soil and vegetation surfaces tend to be warmer than those of the taller vegetation cover; hence, they emit more long-wave radiation. The proportion of energy used to evaporate water from this surface cover is small throughout the entire observation period, rising only to about 30% of the radiant energy input after the spring rains. More energy is involved in the yearly soil heat flux cycle, which is about twice as large as that for the taller surface cover. However, by far the most important energy exchange is the loss of sensible heat to the atmosphere. This flux accounts for more than 70–100% of the net radiant energy input, depending on the time of year.

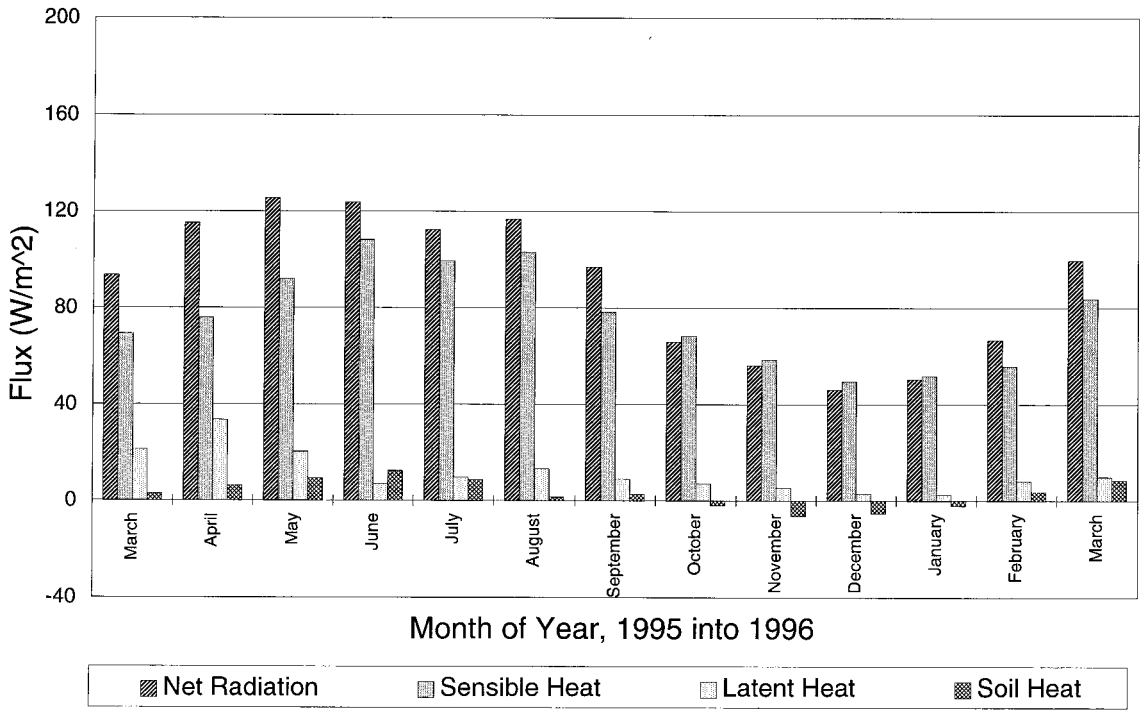

Figure 5. Monthly average values of energy fluxes measured at the short tower at the Rio Rico field site from January 1995 to March 1996

Evaporation from riparian cover classes

Monthly average values of evaporation rate are shown in Figure 6. The values given for tall vegetation and short vegetation are based on measurements (see above) and are assumed to be representative of all type (d) surfaces (i.e. medium/high-density vegetation of medium height) and type (e) surfaces (i.e. low-density, short vegetation) in the riparian system, respectively. Also shown in Figure 6 are the (Penman) potential evaporation and (Shuttleworth) reference crop calculations from January 1995 to March 1996, these being representative of all type (a) covers (i.e. open water surfaces) and type (b) covers (i.e. areas of irrigated agriculture) in the riparian system, respectively.

Both the potential evaporation and reference crop evaporation rates increase steadily from January and peak in June, after which they gently decline through to December. The seasonal behaviour reflects the net input of radiation because both estimation equations have a marked dependence on radiation. The evaporation rates from the taller (mesquite bosque) vegetation show a bimodal pattern, with peaks in March and August. The increasing evaporation rate during January, February, and March is attributable to increasing energy and soil moisture during these months. Because there is little precipitation in May and June, the increasing evaporation is primarily attributable to the increasing energy input, but the evaporation rate peaks in July, August, and September with the advent of the monsoon rainfall. The evaporation rates from shorter, sparse vegetation with bare soil are generally very small throughout the data collection period. However, the rates are somewhat higher in March and April, and this may be attributable to a greater fractional cover of spring vegetation which gradually dies back in the subsequent dry months.

The volumetric rates of evapotranspiration from the river, irrigated crops, mesquite bosque, cottonwood, and short riparian vegetation/bare soil were calculated by multiplying the monthly evaporation rate by the total surface area of the corresponding surface cover in the study reach. Although surface cover area of cottonwood trees (class c) is much less than the surface area of mesquite bosque (class d), the volumetric

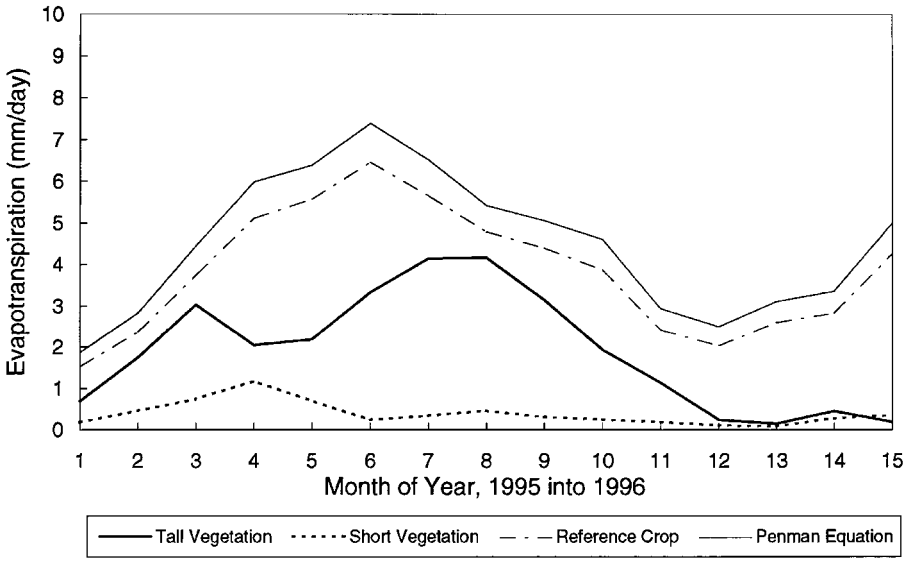

Figure 6. Comparison of evaporation rates in mm day^{-1} from surface water (potential rate), reference crop, tall riparian vegetation, and short vegetation/bare soil tower from January 1995 to March 1996. Values for January and February 1995 for the short tower are scaled with March measurements and tall tower measurements for these two months

evaporation loss from cottonwood is estimated to be similar to that from the tall riparian species because of higher evaporation rate (see section on evaporation from obligatory phreatophytes). The monthly volumetric evaporation rates from the river, irrigated crops, tall riparian vegetation, cottonwood, and short riparian vegetation/bare soil are given in Table II. The equivalent cumulative evaporation volumes for all of 1995 are $4{\cdot}60 \times 10^5$, $6{\cdot}34 \times 10^6$, $2{\cdot}77 \times 10^6$, $2{\cdot}89 \times 10^6$, and $1{\cdot}04 \times 10^6$ m^3, respectively.

CONCLUDING COMMENTS

The micrometeorological measurements at the Rio Rico field site showed the feasibility and, at the same time, the difficulty of obtaining worthwhile measurements and estimates of evaporation for component sur-

Table II. Monthly volumetric evapotranspiration (cubic metres) for January 1995 to March 1996

Month	River	Irrigated crop	Tall vegetation	Cottonwood	Short vegetation and bare soil
January 1995	15 640	205 521	69 849	72 934	37 359
February 1995	21 379	287 548	160 010	167 077	85 582
March 1995	37 219	503 729	307 742	321 333	153 486
April 1995	48 483	665 572	200 829	209 698	233 355
May 1995	53 445	749 549	221 696	231 486	145 565
June 1995	59 896	839 765	327 205	341 655	48 383
July 1995	54 532	760 295	420 109	438 662	70 776
August 1995	45 416	643 430	422 133	440 776	94 849
September 1995	41 037	571 976	309 571	323 242	62 520
October 1995	38 557	521 192	196 388	205 061	51 642
November 1995	23 797	314 587	111 681	116 613	37 432
December 1995	20 910	274 029	24 295	25 368	22 015
January 1996	26 095	349 252	15 185	15 855	17 900
February 1996	25 459	343 359	41 146	42 963	52 591
March 1996	41 736	572 236	19 234	20 083	71 394

face covers in a riparian system in semi-arid environments. The limited area of individual patches of vegetation severely strains the credibility of applying conventional micrometeorological techniques. Fortunately, it was possible to find patches of the two most common cover classes that were sufficiently large that such measurements were adequate, and it was possible to use estimation equations with confidence for two other cover classes.

The use of the energy budget–Bowen ratio method proved worthwhile but problematic. The method works reasonably well when evaporation fluxes are fairly large — during the day over tall riparian vegetation, for example — but the method has important limitations, especially when latent heat fluxes are low and humidity gradients are small. The fact that this weakness could be largely compensated for by the alternative use of the aerodynamic method in this study proved to be critical.

For the tall riparian vegetation, the larger proportion of the radiant energy input to the surface was used to support evaporation, while for short riparian vegetation, most of the energy returns to the atmosphere as sensible heat. Evaporation from short riparian vegetation is always low, while evaporation for tall riparian vegetation can be larger but is strongly dependent on the availability of soil moisture. In terms of the volume of water evaporated from the study reach, the evaporation from irrigated agriculture is very important and accounts for almost half of the total loss. The majority of the remaining evaporation is from the taller riparian vegetation covers, with about one-quarter of the total loss coming from the obligatory phreatophytes, primarily cottonwood.

ACKNOWLEDGEMENTS

Primary support for this study was provided under NASA grant NAG5-3854, with additional support from The University of Arizona and the City of Nogales. Altaf M. Arain was also partially supported by a NASA Global Change Fellowship (NASA Grant NGT-30303), and Paul R. Houser was supported by NASA grant number NAGW-4165. Many fellow students assisted with the research reported here in the context of hydrological field courses carried out at The University of Arizona. In this context, we are grateful to Robert Harrington, Cary White, Faiz Rahman, Mark Williams, Luis Bastidas, and Russell Scott. We are also particularly grateful to Scott Shupe for providing us with the land use map of the Santa Cruz Valley.

REFERENCES

Brutsaert, W. H. 1982. *Evaporation into the Atmosphere*. Kluwer Academic Publishers, Boston.

Desjardins, R. L., Schuepp, P. H., MacPherson, J. I., and Buckley, D. J. 1992. 'Spatial and temporal variations of the fluxes of carbon dioxide and sensible and latent heat over the FIFE site', *J. Geophys. Res.*, **97**(D17), 18467–18475.

Dyer, A. J. and Hicks, B. B. 1970. 'Flux gradient relationships in the constant flux layer', *Q. J. R. Meteorol. Soc.*, **96**, 715–721.

Gatewood, J. S., Robinson, T. W., Colby, B. R., Hem, J. D., and Halpenny, L. C. 1950. 'Use of bottom-land vegetation in the lower Safford Valley, Arizona', *US Geological Survey Water Supply Paper 1103*. USGS, 210 pp.

Kustas, W. P., Goodrich, D. C., Moran, M. S., Amer, A. M., Bach, L. B., Blanford, J. H., Chehbouni, A., Claassen, H., Clements, W. E., Doraiswamy, P. C., Dubois, P., Clarke, T. R., Daughtry, C. S. T., Gellman, D. I., Grant, T. A., Hipps, L. E., Huete, A. R., Humes, K. S., Jackson, T. J., Keefer, T. O., Nichols, W. D., Parry, R., Perry, E. M., Pinker, R. T., Pinter, P. J., Qi, J., Riggs, A. C., Schmugge, T. J., Shutko, A. M., Stannard, D. I., Swiatek, E., van Leeuwen, J. D., van Syl, J., Vidal, A., and Weltz, M. A. 1991. 'An interdisciplinary field study of the energy and water fluxes in the atmosphere-biosphere system over semi-arid rangelands: description and preliminary results', *Bull. Am. Meteor. Soc.*, **72**, 1683–1705.

Penman, H. L. 1948. 'Natural evaporation from open water, bare soil, and grass', *Proc. R. Soc.*, **A193**, 120–145.

Schuepp, P. H., Leclerc, M. Y., MacPherson, J. I., and Desjardins, R. L. 1990. 'Footprint prediction of scalar fluxes from analytical solutions of the diffusion equation', *Boundary-Layer Meteorol.*, **50**, 355–373.

Shuttleworth, W. J. 1993. 'Evaporation', in Maidment, D. R. (Ed.), *Handbook of Hydrology*. McGraw-Hill, Inc., pp. 4.1–4.53.

Stromberg, J. C., Sommerfield, M. R., Patten, D. T., Fry, J., Krama, C., Amalfi, F., and Christian, C. 1993. 'Release of effluent into the Upper Santa Cruz River, Southern Arizona: ecological considerations', in Wallace, M. G. (Ed.), *Proceedings of the Symposium on Effluent Use Management, Tucson, Arizona*. American Water Resources Association, pp. 81–90.

Unland, H. E., Houser, P. R., Shuttleworth, W. J., and Yang, Z-L. 1996. 'Surface flux measurement and modeling at a semi-arid Sonoran Desert site', *J. Agric. For. Meteorol.*, **82**, 119–153.

Webb, E. K. 1970. 'Profile relationships: the log-linear range and extension to strong stability', *Q. J. R. Meteorol. Soc.*, **96**, 67–90.

